Biochem. J. (2015) **467**, 271–280 (Printed in Great Britain) doi:10.1042/BJ20141447

Pyruvate dehydrogenase complex and nicotinamide nucleotide transhydrogenase constitute an energy-consuming redox circuit

Kelsey H. Fisher-Wellman*†, Chien-Te Lin*‡, Terence E. Ryan*‡, Lauren R. Reese*‡, Laura A.A. Gilliam*‡, Brook L. Cathey*‡, Daniel S. Lark*†, Cody D. Smith*‡, Deborah M. Muoio§ and P. Darrell Neufer*†‡[1]

*East Carolina Diabetes and Obesity Institute, East Carolina University, Greenville, NC 27834, U.S.A.
†Department of Kinesiology, East Carolina University, Greenville, NC 27834, U.S.A.
‡Department of Physiology, East Carolina University, Greenville, NC 27834, U.S.A.
§Duke Molecular Physiology Institute, Duke University, Durham, NC 27701, U.S.A.

Cellular proteins rely on reversible redox reactions to establish and maintain biological structure and function. How redox catabolic (NAD^+/NADH) and anabolic ($NADP^+$/NADPH) processes integrate during metabolism to maintain cellular redox homoeostasis, however, is unknown. The present work identifies a continuously cycling mitochondrial membrane potential ($\Delta\Psi_m$)-dependent redox circuit between the pyruvate dehydrogenase complex (PDHC) and nicotinamide nucleotide transhydrogenase (NNT). PDHC is shown to produce H_2O_2 in relation to reducing pressure within the complex. The H_2O_2 produced, however, is effectively masked by a continuously cycling redox circuit that links, via glutathione/thioredoxin, to NNT, which catalyses the regeneration of NADPH from NADH at the expense of $\Delta\Psi_m$. The net effect is an automatic fine-tuning of NNT-mediated energy expenditure to metabolic balance at the level of PDHC. In mitochondria, genetic or pharmacological disruptions in the PDHC–NNT redox circuit negate counterbalance changes in energy expenditure. At the whole animal level, mice lacking functional NNT (C57BL/6J) are characterized by lower energy-expenditure rates, consistent with their well-known susceptibility to diet-induced obesity. These findings suggest the integration of redox sensing of metabolic balance with compensatory changes in energy expenditure provides a potential mechanism by which cellular redox homoeostasis is maintained and body weight is defended during periods of positive and negative energy balance.

Key words: energy balance, energy expenditure, mitochondria, redox buffering.

INTRODUCTION

Numerous pathological conditions ranging from cancer to diabetes are associated with elevated reactive oxygen species [1]. Specific cause and effect relationships in disease aetiology, however, have proven difficult to establish due to the limited mechanistic understanding of redox-regulated control processes *in vivo*. At present, the intracellular redox environment is envisaged as the collection of an estimated 80 000 cysteines within the proteome that undergo reversible redox reactions [2]. The majority (~90 %) of these redox-sensitive cysteines are maintained in a reduced non-equilibrium steady state by the thiol antioxidant redox couples glutathione (GSSG–GSH) and thioredoxin (Trx_{SS}–Trx_{SH}). Disequilibrium between redox couples (i.e. reduction potentials) and thus electron flow is made possible by continuous input into the reductive (NADPH) and oxidative (O_2, H_2O_2) arms of the system, thus giving rise to the term 'redox circuits' [3]. Mitochondria play a central role in this system by providing both a major source of the reductive power (e.g. NADPH) as well as the counterbalance oxidant [e.g. superoxide anion ($O_2\bullet^-$)/H_2O_2] that effectively regulates overall cellular redox charge [4].

Given the potential impact of altered redox homoeostasis in the aetiology and pathology of disease, considerable effort has been directed at identifying the sites and conditions under which $O_2\bullet^-$/H_2O_2 is produced. The electron transport system (ETS) is widely regarded as the principal source of oxidant generation and, in general, conditions that induce a high reduction state in complex I and/or III (e.g. reducing equivalent supply > respiratory demand or inhibition of electron flow) accelerate $O_2\bullet^-$/H_2O_2 production [5]. A number of other mitochondrial enzymes have been identified as sources of oxidant production, including succinate dehydrogenase (complex II) [6], the electron-transferring flavoprotein (ETF)–ubiquinone oxidoreductase [7,8], glycerol-3-phosphate dehydrogenase [9], dihydro-orotate dehydrogenase [9] and the matrix dehydrogenase enzyme complexes α-ketoglutarate dehydrogenase (αKGDH), branched-chain keto-dehydrogenase (BCKDH) and pyruvate dehydrogenase (PDH) [10–15]. The latter three enzyme complexes, all 2-oxoacid dehydrogenases with similar structures and catalytic mechanisms, are particularly intriguing given that each occupy a pivotal position in metabolism.

Experiments using isolated enzyme complex from bovine heart indicate the pyruvate dehydrogenase complex (PDHC) produces H_2O_2 directly at relatively low rates in the presence of both the electron donor (i.e. pyruvate) and the terminal electron acceptor (i.e. NAD^+). However, as the availability of NAD^+ decreases (i.e. NAD^+/NADH increases), H_2O_2 generation increases dramatically [14]. This suggests that PDHC generates H_2O_2 as a function of the overall redox state or 'reducing pressure' within the complex; i.e. the rate of forward electron flux via E1 and E2 relative to the availability of NAD^+. In addition, in intact

Abbreviations: CDNB, 1-chloro-2,4-dinitrobenzene; CrAT, carnitine acetyltransferase; ETS, electron transport system; JH_2O_2, mitochondrial H_2O_2 production rate; JNADH, mitochondrial NADH production rate; JO_2, mitochondrial O_2 consumption rate; NNT, nicotinamide nucleotide transhydrogenase; $O_2\bullet^-$, superoxide; PDHC, pyruvate dehydrogenase complex; TCA, tricarboxylic acid; TPP^+, tetraphenylphosponium; Trx, thioredoxin; VCO_2, rate of carbon dioxide production; VO_2, rate of oxygen consumption; αKGDH, α-ketoglutarate dehydrogenase; $\Delta\Psi_m$, mitochondrial membrane potential.

[1] To whom correspondence should be addressed (email neuferp@ecu.edu).

mitochondria, H_2O_2 production by PDHC increases to extremely high rates as the concentration of the redox buffer GSH declines, suggesting that GSH plays a direct role in buffering the H_2O_2 produced by PDHC [14]. In the present study, the control of PDHC in relation to mitochondrial redox buffering was further explored. PDHC is shown to be part of a continuously cycling redox circuit that links to the NADPH-regenerating, mitochondrial membrane potential ($\Delta\Psi_m$)-dependent, nicotinamide nucleotide transhydrogenase (NNT). This PDHC–NNT circuit reveals a potential novel mechanism by which energy balance is sensed and integrated in real time to generate corresponding reciprocal changes in energy expenditure.

EXPERIMENTAL

Materials

All animal studies were approved by the East Carolina University Institutional Animal Care and Use Committee. C57BL/6N and C57BL/6J mice were purchased from Jackson Laboratory. All mice were housed in a temperature-(22 °C) and light- (12-h light/12-h dark) controlled room and maintained on standard chow with free access to food and water. For all experiments, mice were fasted for 4 h, anaesthetized, and red portions of the gastrocnemius muscle were dissected and separated into fibre bundles in Buffer X (50 mM potassium MES, 7.23 mM potassium EGTA, 2.77 mM calcium potassium EGTA, 20 mM imidazole, 0.5 mM dithiothreitol, 20 mM taurine, 5.7 mM ATP, 14.3 mM phosphocreatine and 6.56 mM $MgCl_2 \cdot 6H_2O$, pH 7.1, 290 mOsm) on ice. Remaining portions of muscle were frozen (liquid N_2) for later analysis. All reagents and chemicals were obtained from Sigma–Aldrich with the exception of Amplex Ultra Red reagent (Invitrogen) and the GSH/GSSG assay kit (Oxis International Inc.).

Permeabilized fibre bundles

Fibre bundles were separated with fine forceps in Buffer X under a dissecting microscope to a single layer of interconnected fibres, permeabilized with 50 μg/ml saponin for 30 min with continuous rotation at 4 °C and washed in ice-cold Buffer Z (110 mM potassium MES, 35 mM KCl, 1 mM EGTA, 5 mM K_2HPO_4, 3 mM $MgCl_2 \cdot 6H_2O$ and 0.5 mg/ml BSA, pH 7.1, 295 mOsm) to remove endogenous substrates. For experiments involving GSH depletion, 1-chloro-2,4-dinitrobenzene (CDNB, 1 μM) or ethanol was added during saponin permeabilization to deplete matrix GSH by ~75 % as previously described [14].

Mitochondrial respiration and H_2O_2 production/emission

High-resolution O_2-consumption measurements were conducted at 37 °C in Buffer Z, supplemented with creatine monohydrate (25 mM), using the Oroboros Oxygraph-2K instruments. Mitochondrial H_2O_2 emission was measured fluorimetrically at 37 °C via Amplex Ultra Red (10 μM)/horseradish peroxidase (3 units/ml) detection system (E_{ex}/E_{em} = 565/600). Fluorescence was monitored using a SPEX Fluoromax 3 (HORIBA Jobin Yvon) spectrofluorimeter with temperature control and magnetic stirring. For each experiment, resorufin fluorescence was converted into nanomolar H_2O_2 via an H_2O_2 standard curve generated under identical substrate conditions as employed for each protocol. Blebbistatin (25 μM) was present during all O_2-consumption and H_2O_2-emission experiments to prevent contraction [16]. At the conclusion of each experiment, fibre bundles were washed in double-distilled water to remove salts, freeze-dried in a lyophilizer (Labconco) and weighed using an Orion Cahn C-35 microbalance (Thermo Electron Corporation).

Mitochondrial NADH production

All NADH-production assays were carried in a potassium phosphate-based buffer (50 mM), containing $CaCl_2$ (10 μM) and $MgCl_2$ (200 μM), pH 7.4. Permeabilized fibres were prepared as indicated above. Following a 15 min wash in Buffer Z, fibres were incubated with the pore-forming peptide alamethicin (30 μg/ml) to permeabilize the inner mitochondrial membrane [11]. Experiments were carried out in the presence of CoA (100 μM), NAD^+ (1 mM), thiamine pyrophosphate (300 μM), rotenone (2 μM) and the indicated substrates. NADH production was tracked via auto fluorescence (E_{ex}/E_{em} = 376/450). Fluorescence values were converted into micromolar NADH via an NADH standard curve.

Mitochondrial membrane potential

Mitochondrial membrane potential ($\Delta\Psi_m$) and respiration rates were measured simultaneously in isolated mitochondria (125 μg of protein/ml) using the Oxygraph-2k combined with electrodes sensitive to tetraphenylphosponium (TPP^+, a membrane-potential-dependent probe) and oxygen at 25 °C. Mitochondria were isolated and pooled from the entire thigh and calf region of mice using a standard isolation protocol [17]. All experiments were run in Buffer Z in the presence of 1.5 μM carboxyatractyloside, 1.25 μg/ml oligomycin, 0.5 mM GDP, 0.1 μM nigericin, 5 μM rotenone and 6 mM succinate. The TPP^+ electrode was calibrated by a five-point titration (1.1–1.7 μM) at the beginning of each experiment. Membrane potential was varied by subsequent titration of the complex II inhibitor malonate (0.25–5 mM). $\Delta\Psi_m$ was calculated from the Nernst equation based on the distribution of TPP^+ using 0.35 mg of protein/μl of matrix volume to correct for non-specific binding of the probe [18]. In the initial experiments (see Figures 4A and 4B), proton conductance was determined during succinate-supported respiration with minimal (2 mM pyruvate) or maximal (2 mM pyruvate + 5 mM carnitine) flux through PDHC. Subsequent experiments (see Figure 4C) also included pyruvate and carnitine plus 10 mM glutamate to induce maximal production of NADH.

GSH measurements

Frozen red gastrocnemius muscle was homogenized in HEPES (3 mM), sucrose (25 mM) and EGTA (0. 5mM), pH 7.2. Buffer was supplemented on the day of experimentation with 1 % Triton and an anti-protease cocktail. Total GSH was measured using the reagents and calibration set provided by the GSH/GSSG assay (Oxis International Inc.).

Whole body calorimetry and body composition

Rates of oxygen consumption (VO_2) and carbon dioxide production (VCO_2), respiratory exchange ratio, food and water intake were measured using a LabMaster System (TSE Systems). Energy expenditure was calculated using the equation [($CVO_2 \times VO_2$) + ($CVCO_2 \times VCO_2$)/1000]. Constants of the equation include: CVO_2 = 3.941 ml/h and $CVCO_2$ = 1.106 ml/h. Infrared sensors were used to record ambulatory activity in 3D axes (x, y, z). Counts across all three axes were summed to give total

ambulatory activity. After 2 days of acclimatization, all rates were averaged over a subsequent 3-day period and expressed per gram of body weight or lean body mass. Fat and lean body mass were determined using an EchoMRI-500 instrument in accordance with the manufacturer's instructions (EchoMRI).

Glucose tolerance

Whole body glucose tolerance was determined from intraperitoneal injection of glucose (1.5 g of glucose/kg of body weight) after a 4-h fast (beginning during the last 3 h of the dark cycle). Blood samples were obtained from tail nick at 0, 30, 60 and 90 min after injection.

Statistics

Data are presented as means ± S.E.M. Statistical analysis was performed using Student's *t* tests or one-way ANOVA with Student–Newman–Keuls methods for analysis of significance among groups. The level of significance was set at $P < 0.05$.

RESULTS

Removal of acetyl-CoA accelerates flux but decreases H_2O_2 production by PDHC in intact mitochondria

Flux through PDHC is inhibited allosterically by acetyl-CoA. Acetyl-CoA accumulates in the mitochondria when production by PDHC (or other enzymes generating acetyl-CoA) exceeds the availability of oxaloacetate and thus limits entry into the TCA (tricarboxylic acid) cycle. In striated muscle, the accumulation of acetyl-CoA is counterbalanced by the activity of carnitine acetyltransferase (CrAT), a mitochondrial enzyme that converts excess acetyl-CoA to membrane-permeant acetylcarnitine esters which then efflux from the organelle and cell (Figure 1A) [19]. To test whether H_2O_2 production by PDHC is directly related to reducing pressure within the complex, a series of experiments were conducted to manipulate flux through the complex using permeabilized skeletal muscle fibre bundles. In agreement with previous findings [19], addition of carnitine during basal respiration supported by pyruvate only (i.e., no malate) increased mitochondrial O_2 consumption (JO_2) and NADH production (JNADH) rates in fibre bundles from wild-type but not muscle-specific $CrAT^{m-/-}$ mice (Figures 1B and 1C), confirming at least partial removal of acetyl-CoA via CrAT accelerates catalytic flux through PDHC [19]. Surprisingly, however, in contrast with the sharp increase in H_2O_2 production rate (JH_2O_2) that occurs when catalytic flux is accelerated through isolated PDHC [14], increased flux induced by addition of carnitine reduced PDHC-mediated JH_2O_2 emission in permeabilized fibres, an effect that was especially evident when mitochondrial GSH was partially depleted by pre-treatment with CDNB (Figure 1D). These findings reveal a clear discrepancy between the control of JH_2O_2 generation in the isolated enzyme [14] compared with intact mitochondria and suggest that the net rate of H_2O_2 production by PDHC in intact mitochondria does not simply reflect a balance between catalytic flux and buffering by GSH.

H_2O_2 generation by PDHC is mitigated by direct coupling to the redox-buffering system

The mitochondrial pools of reduced GSH and Trx2, which regulate and protect protein thiols, are established and maintained by the combined actions of glutathione reductase and thioredoxin reductase (Figure 2A). To determine whether PDHC may be integrated with the mitochondrial redox-buffering system, PDHC-mediated H_2O_2 production was studied in the absence or presence of inhibitors of both glutathione reductase and thioredoxin reductase without depleting matrix GSH. With both arms of the matrix redox-buffering system inhibited, the increase in PDHC catalytic flux induced by carnitine failed to suppress PDHC-mediated JH_2O_2 emission (i.e. pyruvate as the sole substrate); in fact, addition of carnitine generated a marked increase in pyruvate-supported JH_2O_2 emission (Figures 2B and 2C compared with Figure 1D), with the loss of thioredoxin reductase accounting for most of the effect (Figure 2D). The Trx_{SS}–Trx_{SH} redox couple has previously been linked to redox buffering of αKGDH [20], an enzyme complex structurally similar to PDHC. Interestingly, αKGDH is not sensitive to matrix GSH levels [14] but, similar to PDHC, inhibition of thioredoxin reductase increases αKGDH-supported JH_2O_2 emission, particularly when catalytic flux is accelerated by the addition of ADP (results not shown). Collectively, these findings suggest that PDHC and probably the other 2-oxoacid dehydrogenase complexes are capable of generating high rates of H_2O_2, but the net rate of H_2O_2 release is kept in check by direct coupling with the matrix redox-buffering system.

PDHC and NNT are integrated via a continuously cycling redox circuit

The matrix redox-buffering system is regenerated by, and thus derives its reducing power from, NADPH. The principal source of NADPH in the matrix is NNT, an inner mitochondrial transmembrane protein that utilizes the $\Delta\Psi_m$ to drive the reduction in $NADP^+$ from NADH [21]. Thus, NADH is both a substrate for NNT and a source of fuel for the ETS to generate the $\Delta\Psi_m$ needed to support NNT activity.

In the experiments described above, PDHC was the only source of NADH when respiration was supported by pyruvate plus carnitine. It was therefore reasoned that PDHC-derived NADH may contribute to NADPH provision via an NNT-dependent mechanism. This would explain why accelerating flux through PDHC by addition of carnitine reduces JH_2O_2 production when the redox-buffering system is intact (due to increased JNADH production and therefore substrate for NNT; Figure 1D) but increases JH_2O_2 production when the redox-buffering circuit is inhibited (Figure 2C). To test this hypothesis, pyruvate-supported JH_2O_2 emission was measured in permeabilized fibres from C57BL/6J mice, which do not express NNT due to a spontaneous in-frame five exon deletion [22–24] and compared with permeabilized fibres from C57BL/6N mice, which express functional NNT. Similar to the increase in JH_2O_2 production observed when redox buffering was compromised by inhibition of both glutathione and thioredoxin reductase (Figures 2B and 2C), the absence of NNT from C57BL/6J mice resulted in ∼2-fold higher JH_2O_2 emission during respiration supported by pyruvate, which increased to ∼5-fold higher when flux through PDHC was increased by addition of carnitine (Figures 3A and 3B). By contrast, increasing flux through PDHC had no effect on JH_2O_2 emission in fibres from C57BL/6N mice, indicating that continuous regeneration of NADPH via NNT is critical to buffering the H_2O_2 produced by PDHC. In fibres lacking NNT, providing an alternative means of regenerating NADPH via NADP-linked isocitrate dehydrogenase (i.e. increased flux of acetyl-CoA into the TCA cycle via addition of malate) during maximal flux through PDHC reduced H_2O_2 emission back to baseline (Figure 3C), indicating restoration of the buffering network. Subsequent inhibition of glutathione and thioredoxin reductases reversed the effect of malate, confirming

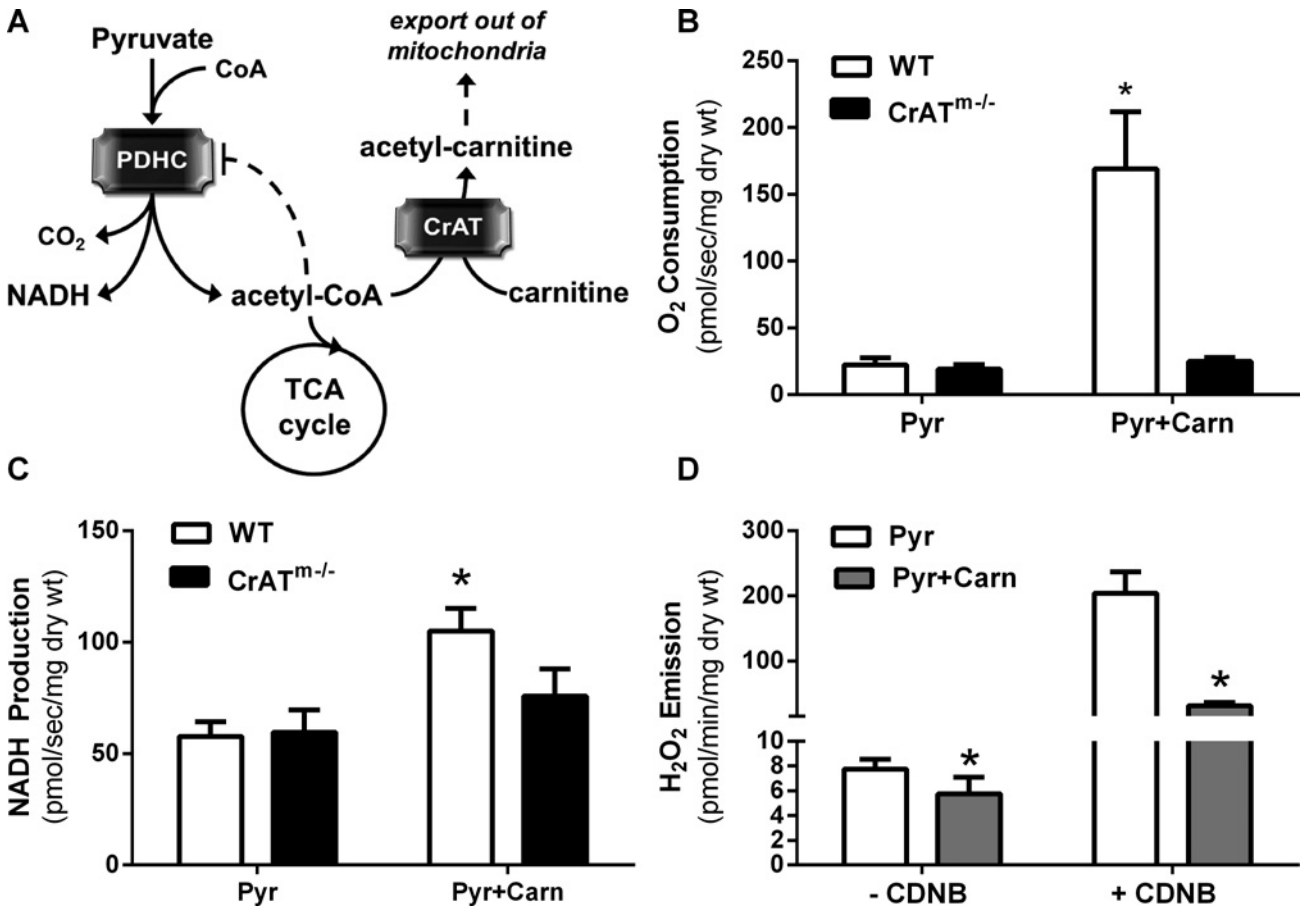

Figure 1 Effect of carnitine on PDHC flux and H_2O_2 emission

Permeabilized fibre bundles were prepared from red portions of the gastrocnemius muscle. (**A**) Schematic diagram showing product inhibition of PDHC by acetyl-CoA and removal of acetyl-CoA via CrAT in the presence of carnitine [28]. (**B**) JO_2 in permeabilized skeletal muscle fibre bundles from C57BL/6N wild-type (WT) and muscle-specific CrAT-knockout ($CrAT^{m-/-}$) mice during respiration supported by pyruvate or pyruvate plus carnitine. (**C**) Rate of NADH production under the same experimental conditions as in (**B**). Fibres were pre-treated with alamethicin (30 μg/ml) to permeabilize mitochondria prior to assay. (**D**) Mitochondrial H_2O_2 emission rate during respiration supported by pyruvate or pyruvate plus carnitine in fibres from WT mice $\pm$ pre-treatment with CDNB (1 μM during permeabilization) to partially deplete (~75 %) mitochondrial GSH [14].

that the effect of malate was mediated via restoration of NADPH synthesis. These findings emphasize the dependence of PDHC on an NNT-linked redox-buffering network to regulate the net H_2O_2 emission by PDHC.

PDHC produces H_2O_2 continuously

The experiments described above were carried out under non-ADP-stimulated conditions (i.e. low demand). To determine whether H_2O_2 is produced by PDHC in a more physiological context, JH_2O_2 was followed in response to titration of ADP in fibres from C57BL/6J mice supported by pyruvate plus carnitine. Titration of ADP led to a dose-dependent decrease in JH_2O_2 emission (Figure 3D), presumably reflecting a progressive increase in the oxidation rate of NADH. Interestingly, however, even during maximal respiration, the rate of H_2O_2 production was considerably higher in fibres from C57BL/6J (~22 pmol/min/mg of dry weight) compared with C57BL/6N (<5 pmol/min/mg of dry weight) mice. However, when redox buffering was blocked in fibres from C57BL/6N mice (as in Figure 2), JH_2O_2 production during maximum ADP-stimulated respiration was similar (~18 pmol/min/mg of dry weight) to that seen in fibres from C57BL/6J mice. Taken together, these findings suggest that PDHC produces H_2O_2 continuously, even under ADP-stimulated conditions, but that production is effectively masked by a membrane-potential-dependent redox circuit that couples PDHC-mediated NADH production with NNT-mediated NADPH regeneration, thereby regulating the net rate of H_2O_2 release from PDHC.

PDHC–NNT constitute an energy-consuming redox circuit

The fact that NNT-mediated NADPH generation consumes $\Delta\Psi_m$ suggests that continuous flux through NNT-linked redox circuits contributes to energetic demand [25]. To directly test this hypothesis, JO_2 was measured as a function of $\Delta\Psi_m$ under conditions designed to stimulate maximal H_2O_2 production and thus demand on NNT activity. In these experiments, a higher JO_2 for a given $\Delta\Psi_m$ reflects a greater rate of proton conductance across the inner mitochondrial membrane and generates a leftward shift in the curve [5].

Figure 4(A) shows data from mitochondria isolated from C57BL/6N mice (i.e. NNT intact). With the substrate combination of succinate + pyruvate + carnitine, the highest membrane potential achieved (145 mV) is associated with a JO_2 of 239 pmol/s/mg. By contrast, with succinate or succinate + pyruvate as substrates, the same membrane potential (145

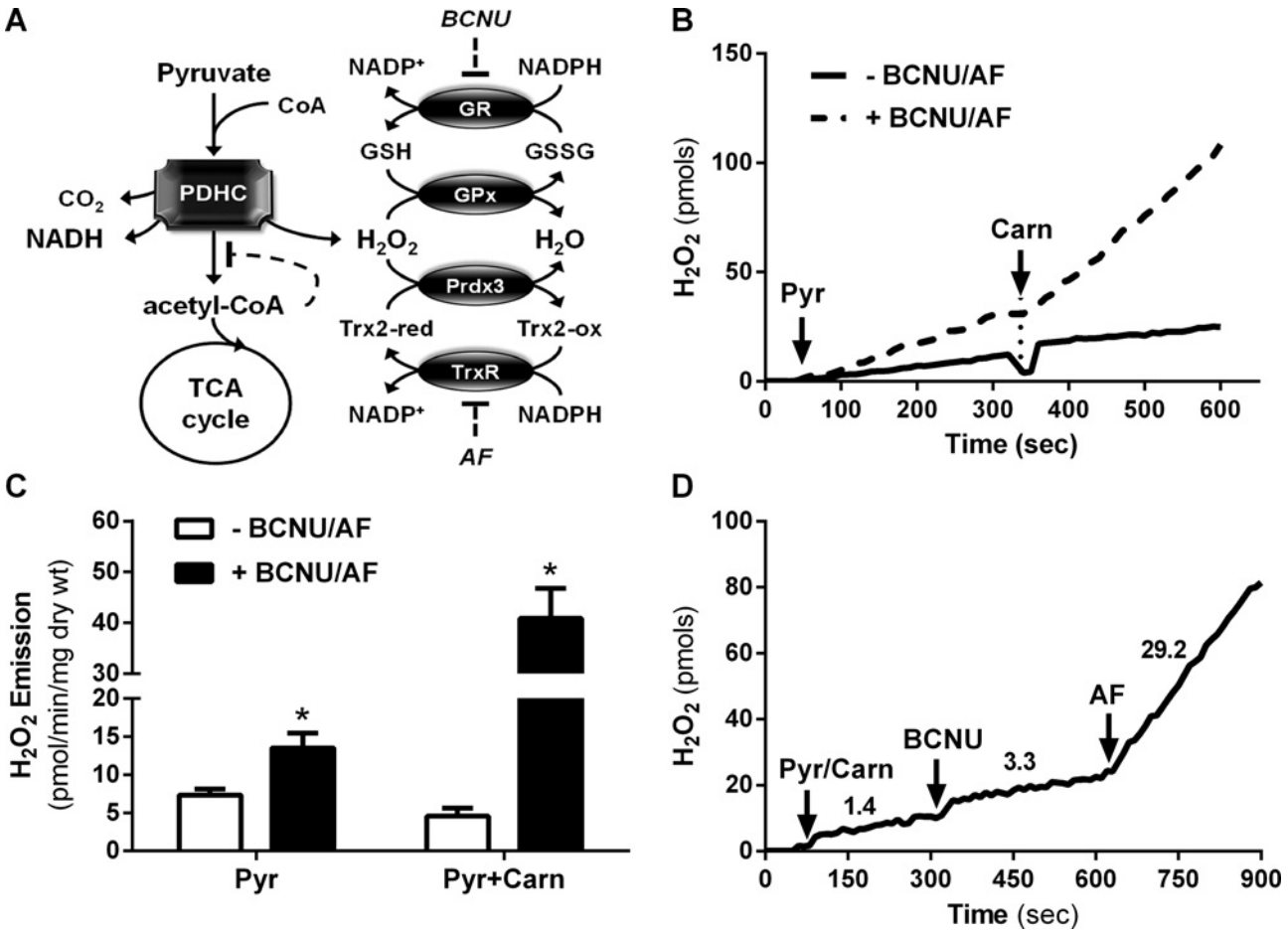

Figure 2 Effect of inhibiting matrix redox buffering on H_2O_2 emission by PDHC

(**A**) Schematic diagram showing the glutathione and peroxiredoxin/thioredoxin H_2O_2-buffering circuits. GPx, glutathione peroxidase; GR, glutathione reductase; Prdx3, mitochondrial peroxiredoxin; Trx2, mitochondrial thioredoxin shown in reduced and oxidized forms; TrxR, thioredoxin reductase. (**B**) Representative trace of mitochondrial H_2O_2 emission in response to sequential addition of pyruvate and carnitine in the presence or absence of inhibitors of GR [bis-chloroethylnitrosourea (BCNU)] and TrxR [auranofin (AF)]. (**C**) Quantified H_2O_2-emission rates from experiments in (**D**). (**D**) Representative trace of JH_2O_2 emission in response to sequential addition of pyruvate/carnitine (Pyr/Carn), BCNU and AF. Data are expressed as means ± S.E.M., $n = 6$–12 per experiment, $^*P < 0.05$.

mV) is associated with a significantly lower JO_2 (150–160 pmol/s/mg), indicating that inclusion of carnitine accelerates proton conductance, consistent with an increased rate of flux through PDHC (due to carnitine-catalysed removal of acetyl-CoA), increased JH_2O_2 production and increased flux through the NNT redox circuit.

Figure 4(B) shows identical experiments conducted on mitochondria isolated from C57BL/6J mice. The three substrate conditions generate identical curves, indicating no difference in proton conductance. This finding is consistent with the fact that C57BL/6J mice lack NNT and therefore lack the capacity to increase proton conductance when flux through PDHC is elevated by the presence of carnitine. Thus, the measured net JH_2O_2 is markedly higher (Figures 3A and 3B) because the mechanism that normally buffers the H_2O_2 is absent. In C57BL/6N mice, the same JH_2O_2 rate is generated but is masked by cycling of the redox-buffering circuit (Figures 3B, 3C and 4A).

Figure 4(C) shows data in which proton-conductance experiments were repeated to provide a direct comparison between mitochondria isolated from C57BL/6N compared with C57BL/6J mice. Again, at the highest common $\Delta\Psi_m$ (142 mV), JO_2 was much higher in mitochondria from C57BL/6N than C57BL/6J mice (231 compared with 102 pmol/s/mg). Glutamate was included as a substrate in these experiments in an attempt to also maximize JH_2O_2 production from complex I and/or αKGDH; however, the impact on proton conductance over succinate + pyruvate + carnitine was minimal (results not shown). Collectively, these findings suggest that PDHC, as well as other sources of H_2O_2, link through redox-buffering systems to NNT to form continuously cycling energy-consuming redox circuits.

Mice lacking NNT have lower energy expenditure

The establishment and maintenance of a relatively reduced redox environment throughout the mitochondrial and cellular proteome depends on the continuous generation of NADPH, implying that NNT activity may represent a significant source of energy expenditure. NNT, similar to other proteins/processes requiring an input of energy (e.g. ATP synthase, adenine nucleotide translocase or calcium uptake), consumes $\Delta\Psi_m$ to drive its activity. From a whole organism perspective, a greater rate of O_2 consumption corresponds to a greater rate of $\Delta\Psi_m$ dissipation (i.e. higher demand), whereas reduced O_2 consumption reflects a lower rate of $\Delta\Psi_m$ dissipation (i.e. lower demand). In mice lacking functional NNT (C57BL/6J), rates of whole body O_2 consumption, CO_2

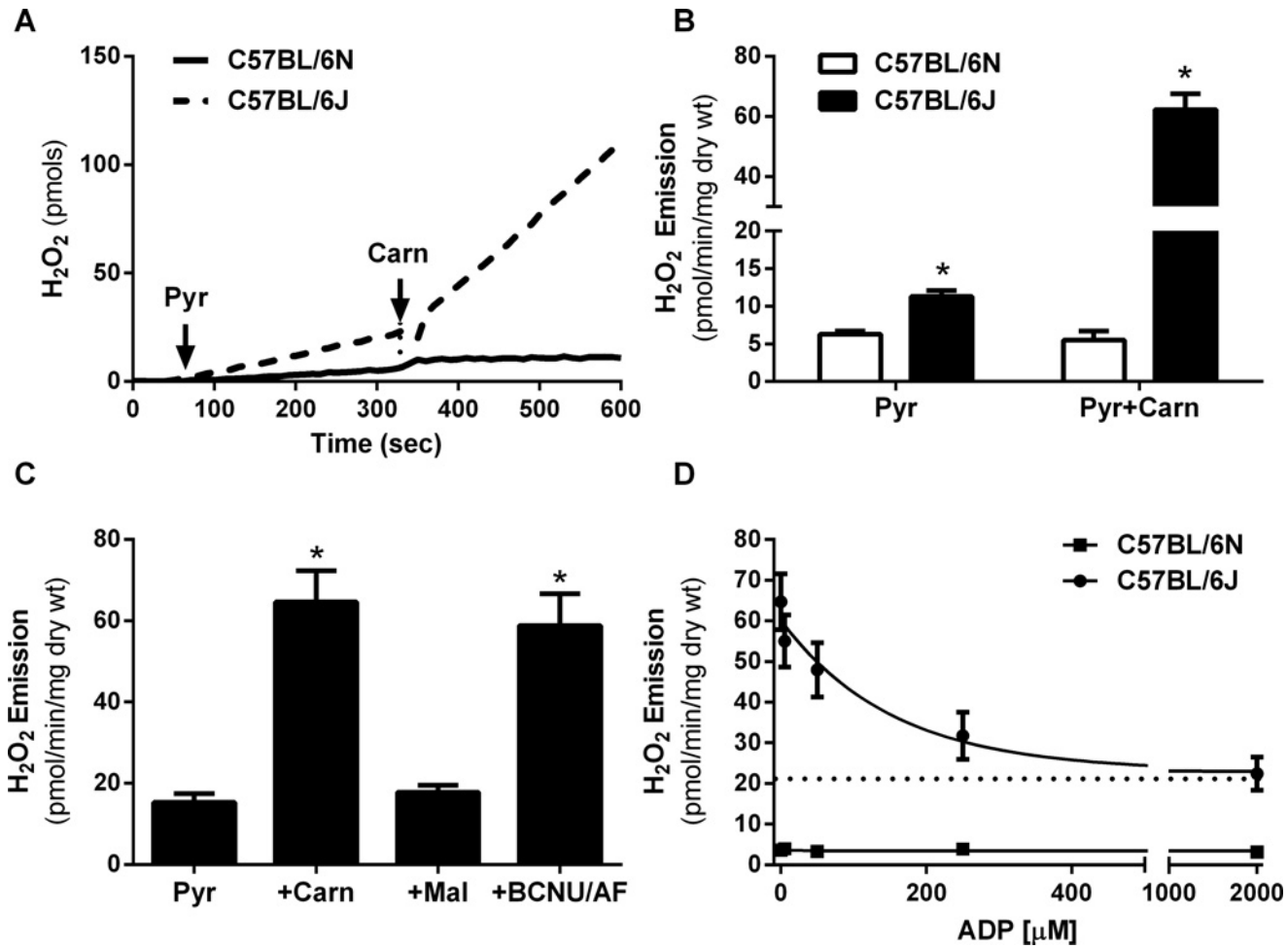

Figure 3 Comparison of H_2O_2 production by PDHC in mitochondria from C57BL/6N compared with C57BL/6J mice

(**A**–**D**) Permeabilized fibre bundles were prepared from red portions of the gastrocnemius muscle from C57BL/6N (6N) or C57BL/6J (6J) mice. (**A**) Representative trace of H_2O_2 emission during respiration supported by sequential addition of pyruvate (Pyr) and carnitine (Carn) in fibres from 6N (+ NNT) compared with 6J (− NNT) mice. (**B**) Quantified H_2O_2 emission rates from experiments in (**A**). (**C**) Rates of H_2O_2 emission in fibres from 6J (− NNT) mice in response to sequential addition of pyruvate, carnitine, malate (Mal) and the glutathione/thioredoxin reductase inhibitors [bis-chloroethylnitrosourea (BCNU) and auranofin (AF) respectively]. (**D**) Pyruvate (1 mM) and carnitine (5 mM)-supported H_2O_2 emission in response to increasing concentrations of ADP (0, 5, 50, 500 and 2000 μM). Assay buffer was supplemented with hexokinase (1 unit/ml) and 2-deoxyglucose (5 mM) to clamp ADP at each desired concentration.

production (results not shown) and energy expenditure were lower than in mice with NNT intact (C57BL/6N), whether normalized to total body mass (Figures 5A and 5B) or fat-free mass (Figures 5C and 5D). Total activity, food intake on a standard diet and respiratory exchange ratio were identical between the two strains (results not shown) and thus could not account for the difference in energy expenditure. Mice lacking NNT were also characterized by a higher percentage of body fat (Figure 5E) and, consistent with previous reports [22,23], lower glucose tolerance (Figure 5F). Although the C57BL/6J strain also displays impaired insulin secretion and harbours a number of other genetic mutations [22,23], the current findings provide evidence that NNT activity is a significant contributor to whole body energy expenditure, the absence of which probably contributes to the increased susceptibility of the widely used C57BL/6J strain to diet-induced obesity and insulin resistance.

DISCUSSION

The present study reveals a continuously cycling redox circuit between PDHC and NNT. PDHC produces H_2O_2 at substantial rates as a natural by-product of catalysis, even under conditions when the 'reducing pressure' within the complex is minimal (i.e. high NAD^+ availability and ADP-stimulated respiration). Under normal circumstances, the H_2O_2 is reduced to H_2O and is thus masked by the cycling of the redox circuit. The reducing power for the circuit is derived from and dependent upon the continuous regeneration of NADPH via NNT and the flow of electrons through the GSH and/or Trx redox couples. Because NNT activity is dependent on $\Delta\Psi_m$, electron flux through the PDHC–NNT circuit comes at the expense of energy. The greater the rate of H_2O_2 production by PDHC, the greater the rate of NNT activity and thus energy utilization (Figure 6).

To our knowledge, the PDHC–NNT circuit is the first intact continuously cycling redox circuit to be identified, although it is likely to be representative of redox circuits functioning throughout the proteome. In the context of redox biology, cells evolved to integrate redox catabolic (NAD^+/NADH) and anabolic ($NADP^+$/NADPH) processes to generate and maintain an optimal 'redox charge' against the default pressure of oxidation imposed by the environment. The majority of redox-sensitive thiols in the proteome are maintained in a reduced state by virtue of the thermodynamics of the reductive system dominating over the

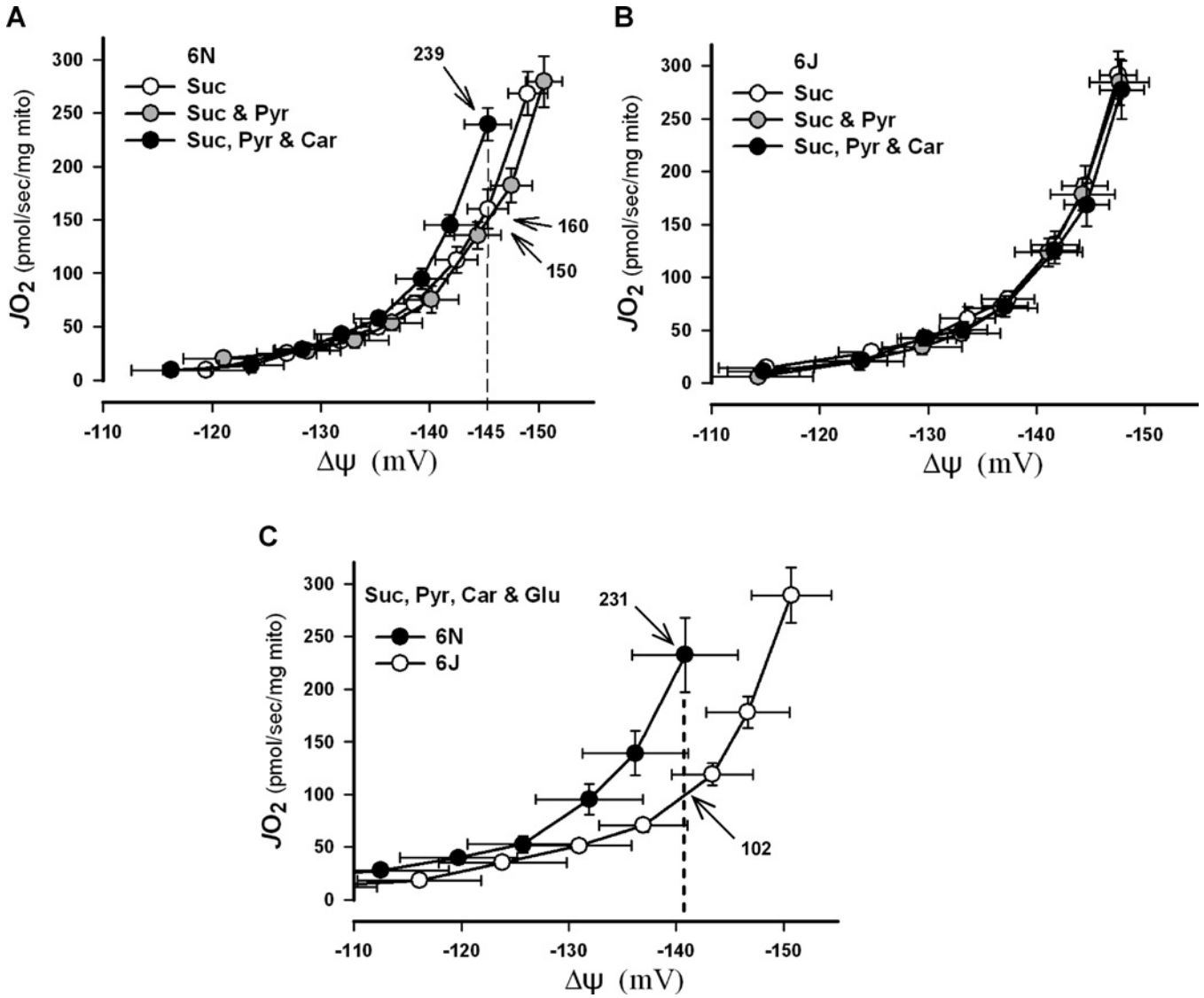

Figure 4 Effect of accelerating flux through the PDHC–NNT circuit on mitochondrial proton conductance

(**A**–**C**) Mitochondria were isolated from gastrocnemius and quadriceps muscle from C57BL/6N or C57BL/6J mice. (**A** and **B**) Rates of O_2 consumption as a function of $\Delta\Psi_m$ in mitochondria isolated from C57BL/6N (+ NNT; **A**) and C57BL/6J (− NNT; **B**) mice during respiration with minimal (succinate and succinate + pyruvate) and maximal (succinate + pyruvate + carnitine) flux through PDHC. Note the differences in JO_2 (numbers with arrows) at a given $\Delta\Psi_m$ (dotted line) indicating differences in proton conductance. (**C**) Direct comparison of proton conductance in isolated mitochondria from C57BL/6N and C57BL/6J mice under substrate conditions inducing maximal H_2O_2 production from PDHC and complex I (succinate + pyruvate + carnitine + glutamate). Note greater proton conductance in C57BL/6N mice at the highest common $\Delta\Psi_m$. Car, carnitine; Glu, glutamate; Pyr, pyruvate; Suc, succinate.

relatively low rate of non-enzymatic protein thiol oxidation. The mid-point potentials for the NAD and NADP redox couples are virtually identical, which means the equilibrium constant for the reaction catalysed by NNT,

$$NADH + NADP^+ \leftrightarrow NAD^+ + NADPH$$

should be ∼1 [26]. However, the reaction is maintained far from its theoretical equilibrium by $\Delta\Psi_m$ which drives the reaction far to the right, generating a highly reduced $NADP^+$/NADPH redox state. The mitochondrial and cytosolic NADP(H) redox states are maintained in equilibrium by the NADP-linked α-ketoglutarate/isocitrate redox shuttle, thus ensuring the reducing power of the mitochondria (i.e. 'electrical charge') is distributed and held via GSH- and Trx-dependent systems throughout the redox proteome. Analogous to the activation of ATP synthase in response to increased cellular ATPase activity, an increase in the oxidation rate of specific protein thiols anywhere in the cell will instantly draw electrons from the GSH and/or Trx redox-buffering circuits, ultimately 'pulling current' from NADPH at the expense of NNT-mediated energy expenditure. This suggests (1) that control of the redox environment is exerted and dominated by the kinetics of the reductive arm of the system rather than simply by the production of reactive oxygen species, and (2) that preservation of mitochondrial content (i.e. 'reducing power'), particularly in the context of disease, aging, etc., is critical to sustaining a stable redox environment.

PDHC occupies a pivotal position in metabolism, raising the question as to why the complex may have evolved to produce H_2O_2 directly. One possibility is that the PDHC–NNT circuit is uniquely positioned in intermediary metabolism to

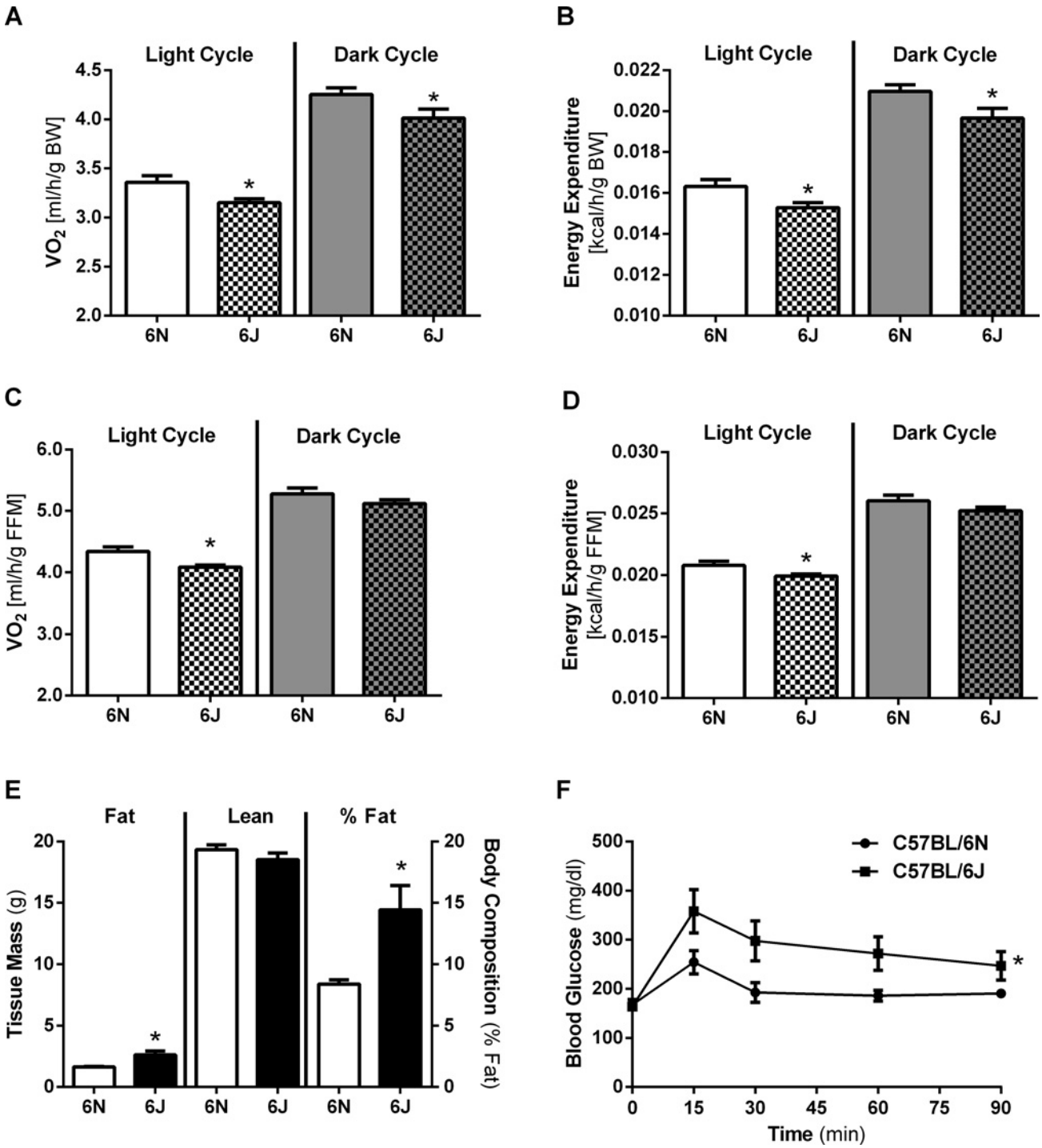

Figure 5 Mice lacking NNT have lower energy expenditure and glucose tolerance

(**A**–**D**) Indirect metabolic calorimetry in C57BL/6N (6N) and C57BL/6J (6J) mice. (**A**) Oxygen consumption and (**B**) calculated energy expenditure per gram of body mass (BW). (**C**) Oxygen consumption and (**D**) calculated energy expenditure per gram of fat free mass (FFM). *Different from 6N mice within either the light or the dark cycle ($P < 0.05$), n=10–13/group. (**E**) Fat mass, lean body mass, percentage fat mass and (**F**) whole body glucose tolerance determined in 6N and 6J mice at ~10–12 weeks of age. Data are means ± S.E.M., $n = 10$/group. *Different from 6N ($P < 0.05$), n=10/group.

provide a safeguard against imbalances imposed on the system. When energy supply exceeds energy demand, the increased 'reducing pressure' (i.e. increased NADH/NAD^+, more negative reduction potential) on the ETS and therefore tendency to increase $\Delta\Psi_m$ and NADPH/$NADP^+$ is counterbalanced by the increase in PDHC-mediated H_2O_2 production and acceleration of flux through the PDHC–NNT circuit. This bilateral function protects against the potential for hyper-reduction in the proteome while simultaneously increasing the rate of energy expenditure and thereby at least partially compensating for the surplus energy.

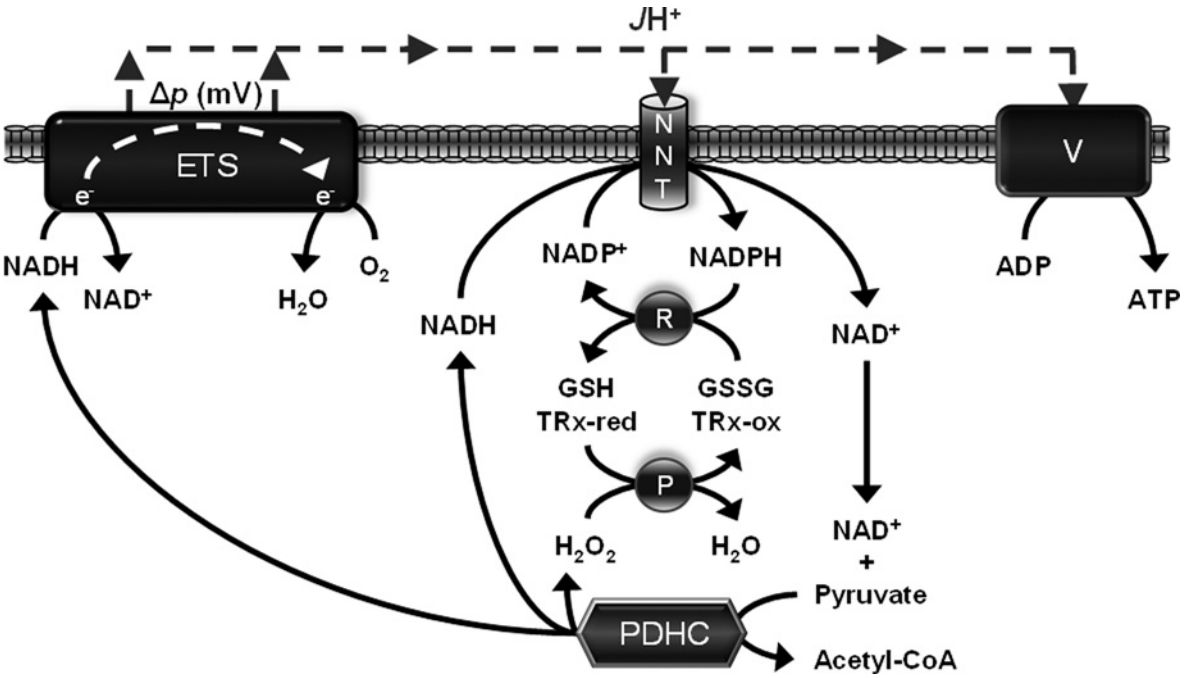

Figure 6 Schematic illustration of the PDHC–NNT redox circuit

The proposed model shows the integration of PDHC with both the ETS and the NNT-linked redox-buffering circuit, providing a mechanism by which redox control processes regulate energy balance. P in circle represents matrix peroxidases and R in circle represents matrix reductases; ox, oxidized; red, reduced; V, complex V (ATP synthase).

Interestingly, in humans, active periods of weight gain due to excess caloric intake induce a much greater than predicted (prediction based on thermic effect of food and change in metabolic mass [24]) increase in resting energy expenditure rate, whereas active periods of weight loss due to caloric restriction induce a much lower than predicted decrease in resting energy expenditure rate [27]. The integration of redox control processes with energy utilization, as exemplified by the PDHC–NNT circuit, provides a potential mechanism for these compensatory changes in energy expenditure/efficiency that defend normal body weight [27], offering a possible new avenue for therapeutic development to treat obesity and other weight-management conditions.

AUTHOR CONTRIBUTION

Kelsey Fisher-Wellman, Chien-Te Lin, Deborah Muoio and Darrell Neufer conceived and designed the experiments. Kelsey Fisher-Wellman, Chien-Te Lin, Terence Ryan, Lauren Reese, Laura Gilliam, Brook Cathey, Daniel Lark and Cody Smith performed the experiments. Kelsey Fisher-Wellman, Chien-Te Lin and Darrell Neufer analysed the data. Kelsey Fisher-Wellman and Darrell Neufer wrote the manuscript.

FUNDING

This work was supported by the U. S. Public Health Service [grant numbers F32 AR061946 (to L.A.A.G.), R01 DK089312 (to D.M.M.), R01 DK073488 and R01 DK096907 (to P.D.N.)].

REFERENCES

1 Valko, M., Leibfritz, D., Moncol, J., Cronin, M.T., Mazur, M. and Telser, J. (2007) Free radicals and antioxidants in normal physiological functions and human disease. Int. J. Biochem. Cell Biol. **39**, 44–84 CrossRef PubMed
2 Go, Y.-M. and Jones, D.P. (2013) The redox proteome. J. Biol. Chem. **288**, 26512–26520 CrossRef PubMed
3 Jones, D.P. and Go, Y.-M. (2011) Mapping the cysteine proteome: analysis of redox-sensing thiols. Curr. Opin. Chem. Biol. **15**, 103–112 CrossRef PubMed
4 Fisher-Wellman, K.H. and Neufer, P.D. (2012) Linking mitochondrial bioenergetics to insulin resistance via redox biology. Trends Endocrinol. Metab. **23**, 142–153 CrossRef PubMed
5 Divakaruni, A.S. and Brand, M.D. (2011) The regulation and physiology of mitochondrial proton leak. Physiology **26**, 192–205 CrossRef PubMed
6 Quinlan, C.L., Orr, A.L., Perevoshchikova, I.V., Treberg, J.R., Ackrell, B.A. and Brand, M.D. (2012) Mitochondrial complex II can generate reactive oxygen species at high rates in both the forward and reverse reactions. J. Biol. Chem. **287**, 27255–27264 CrossRef PubMed
7 Perevoshchikova, I.V., Quinlan, C.L., Orr, A.L., Gerencser, A.A. and Brand, M.D. (2013) Sites of superoxide and hydrogen peroxide production during fatty acid oxidation in rat skeletal muscle mitochondria. Free Radic. Biol. Med. **61**, 298–309 CrossRef PubMed
8 Watmough, N.J. and Frerman, F.E. (2010) The electron transfer flavoprotein: ubiquinone oxidoreductases. Biochim. Biophys. Acta **1797**, 1910–1916 CrossRef PubMed
9 Orr, A.L., Quinlan, C.L., Perevoshchikova, I.V. and Brand, M.D. (2012) A refined analysis of superoxide production by mitochondrial sn-glycerol 3-phosphate dehydrogenase. J. Biol. Chem. **287**, 42921–42935 CrossRef PubMed
10 Ambrus, A. and Adam-Vizi, V. (2013) Molecular dynamics study of the structural basis of dysfunction and the modulation of reactive oxygen species generation by pathogenic mutants of human dihydrolipoamide dehydrogenase. Arch. Biochem. Biophys. **538**, 145–155 CrossRef PubMed
11 Starkov, A.A., Fiskum, G., Chinopoulos, C., Lorenzo, B.J., Browne, S.E., Patel, M.S. and Beal, M.F. (2004) Mitochondrial alpha-ketoglutarate dehydrogenase complex generates reactive oxygen species. J. Neurosci. **24**, 7779–7788 CrossRef PubMed
12 Bunik, V.I. and Sievers, C. (2002) Inactivation of the 2-oxo acid dehydrogenase complexes upon generation of intrinsic radical species. Eur. J. Biochem. **269**, 5004–5015 CrossRef PubMed
13 Tretter, L. and Adam-Vizi, V. (2004) Generation of reactive oxygen species in the reaction catalyzed by alpha-ketoglutarate dehydrogenase. J. Neurosci. **24**, 7771–7778 CrossRef PubMed
14 Fisher-Wellman, K.H., Gilliam, L.A., Lin, C.T., Cathey, B.L., Lark, D.S. and Neufer, P.D. (2013) Mitochondrial glutathione depletion reveals a novel role for the pyruvate dehydrogenase complex as a key H_2O_2-emitting source under conditions of nutrient overload. Free Radic. Biol. Med. **65**, 1201–1208 CrossRef PubMed
15 Quinlan, C.L., Goncalves, R.L., Hey-Mogensen, M., Yadava, N., Bunik, V.I. and Brand, M.D. (2014) The 2-oxoacid dehydrogenase complexes in mitochondria can produce superoxide/hydrogen peroxide at much higher rates than complex I. J. Biol. Chem. **289**, 8312–8325 CrossRef PubMed

16 Perry, C.G., Kane, D.A., Lin, C.T., Kozy, R., Cathey, B.L., Lark, D.S., Kane, C.L., Brophy, P.M., Gavin, T.P., Anderson, E.J. and Neufer, P.D. (2011) Inhibiting myosin-ATPase reveals a dynamic range of mitochondrial respiratory control in skeletal muscle. Biochem. J. **437**, 215–222 CrossRef PubMed
17 Frezza, C., Cipolat, S. and Scorrano, L. (2007) Organelle isolation: functional mitochondria from mouse liver, muscle and cultured fibroblasts. Nat. Protoc. **2**, 287–295 CrossRef PubMed
18 Affourtit, C., Quinlan, C.L. and Brand, M.D. (2012) Measurement of proton leak and electron leak in isolated mitochondria. Methods Mol. Biol. **810**, 165–182 CrossRef PubMed
19 Muoio, D.M., Noland, R.C., Kovalik, J.P., Seiler, S.E., Davies, M.N., DeBalsi, K.L., Ilkayeva, O.R., Stevens, R.D., Kheterpal, I., Zhang, J. et al. (2012) Muscle-specific deletion of carnitine acetyltransferase compromises glucose tolerance and metabolic flexibility. Cell Metab. **15**, 764–777 CrossRef PubMed
20 Bunik, V.I. (2003) 2-Oxo acid dehydrogenase complexes in redox regulation. Eur. J. Biochem. **270**, 1036–1042 CrossRef PubMed
21 Hoek, J.B. and Rydstrom, J. (1988) Physiological roles of nicotinamide nucleotide transhydrogenase. Biochem. J. **254**, 1–10 PubMed
22 Freeman, H.C., Hugill, A., Dear, N.T., Ashcroft, F.M. and Cox, R.D. (2006) Deletion of nicotinamide nucleotide transhydrogenase: a new quantitive trait locus accounting for glucose intolerance in C57BL/6J mice. Diabetes **55**, 2153–2156 CrossRef PubMed
23 Toye, A.A., Lippiat, J.D., Proks, P., Shimomura, K., Bentley, L., Hugill, A., Mijat, V., Goldsworthy, M., Moir, L., Haynes, A. et al. (2005) A genetic and physiological study of impaired glucose homeostasis control in C57BL/6J mice. Diabetologia **48**, 675–686 CrossRef PubMed
24 Ronchi, J.A., Figueira, T.R., Ravagnani, F.G., Oliveira, H.C., Vercesi, A.E. and Castilho, R.F. (2013) A spontaneous mutation in the nicotinamide nucleotide transhydrogenase gene of C57BL/6J mice results in mitochondrial redox abnormalities. Free Radic. Biol. Med. **63**, 446–456 CrossRef PubMed
25 Lopert, P. and Patel, M. (2014) Nicotinamide nucleotide transhydrogenase (Nnt) links the substrate requirement in brain mitochondria for hydrogen peroxide removal to the thioredoxin/peroxiredoxin (Trx/Prx) system. J. Biol. Chem. **289**, 15611–15620 CrossRef PubMed
26 Houtkooper, R.H., Canto, C., Wanders, R.J. and Auwerx, J. (2010) The secret life of NAD + : an old metabolite controlling new metabolic signaling pathways. Endocr. Rev. **31**, 194–223 CrossRef PubMed
27 Leibel, R.L., Rosenbaum, M. and Hirsch, J. (1995) Changes in energy expenditure resulting from altered body weight. N. Engl. J. Med. **332**, 621–628 CrossRef PubMed
28 Noland, R.C., Koves, T.R., Seiler, S.E., Lum, H., Lust, R.M., Ilkayeva, O., Stevens, R.D., Hegardt, F.G. and Muoio, D.M. (2009) Carnitine insufficiency caused by aging and overnutrition compromises mitochondrial performance and metabolic control. J. Biol. Chem. **284**, 22840–22852 CrossRef PubMed

Received 26 November 2014/23 January 2015; accepted 3 February 2015
Published as BJ Immediate Publication 3 February 2015, doi:10.1042/BJ20141447